Controlled Tau Cleavage in Cells Reveals Abnormal Localizations of Tau Fragments

Anne Fourest-Lieuvin, Angélique Vinit, Béatrice Blot, Anthime Perrot, Eric Denarier, Frédéric Saudou, Isabelle Arnal

NEUROSCIENCE
RESEARCH ARTICLE

A. Fourest-Lieuvin et al. / Neuroscience xxx (2022) xxx–xxx

Controlled Tau Cleavage in Cells Reveals Abnormal Localizations of Tau Fragments

Anne Fourest-Lieuvin, * Angélique Vinit † Béatrice Blot Anthime Perrot, Eric Denarier, Frédéric Saudou and Isabelle Arnal *

Université Grenoble Alpes, INSERM, U1216, CEA, CNRS, CHU Grenoble Alpes, Grenoble Institut Neurosciences, 38000 Grenoble, France

Abstract—In several forms of dementia, such as Alzheimer's disease, the cytoskeleton-associated protein tau undergoes proteolysis, giving rise to fragments that have a toxic impact on neuronal homeostasis. How these fragments interact with cellular structures, in particular with the cytoskeleton, is currently incompletely understood. Here, we developed a method, derived from a Tobacco Etch Virus (TEV) protease system, to induce controlled cleavage of tau at specific sites. Five tau proteins containing specific TEV recognition sites corresponding to pathological proteolytic sites were engineered, and tagged with GFP at one end and mCherry at the other. After a controlled cleavage to produce GFP-N-terminal and C-terminal-mCherry fragments, we followed the fate of tau fragments in cells. Our results showed that whole engineered tau proteins associate with the cytoskeleton similarly to the non-modified tau, whereas tau fragments adopted different localizations with respect to the actin and microtubule cytoskeletons. These distinct localizations were confirmed by expressing each separate fragment in cells. Some cleavages – in particular cleavages at amino-acid positions 124 or 256 – displayed a certain level of cellular toxicity, with an unusual relocalization of the N-terminal fragments to the nucleus. Based on the data presented here, inducible cleavage of tau by the TEV protease appears to be a valuable tool to reproduce tau fragmentation in cells and study the resulting consequences on cell physiology.

Key words: Tau, Protein cleavage, TEV protease, Microtubule, Actin, nucleus.

INTRODUCTION

Tau is a neuronal protein initially identified as a microtubule-associated protein (MAP) able to stabilize and bundle microtubules (Weingarten et al., 1975; Cleveland et al., 1977a; 1977b; Chen et al., 1992; Kanai et al., 1992; Takemura et al., 1992; Samsonov et al., 2004; Prezel et al., 2018). In addition to its microtubule-binding activity, tau was shown to bind and regulate actin filaments *in vitro* and in cells, including neuronal cells (Correas et al., 1990; Moraga et al., 1993; Kempf et al., 1996; Yu and Rasenick, 2006; Fulga et al., 2007; He et al., 2009; Frandemiche et al., 2014; Elie et al., 2015). Tau can also promote co-organization of actin filaments and microtubules (Farias et al., 2002; Elie et al., 2015; Cabrales Fontela et al., 2017; Biswas and Kalil, 2018). Hence, tau is of primary importance for cytoskeleton homeostasis and organization in neurons (Kapitein and Hoogenraad, 2015; Guo et al., 2017).

In the human central nervous system, the gene encoding tau (*MAPT*) undergoes alternative splicing to produce six different isoforms. These isoforms differ in the presence of the N-terminal inserts N1 and N2 and the second repeat domain R2. The 2N4R isoform is the longest, with 441 amino-acids, whereas the 1N4R and 1N3R isoforms are the most abundant tau species in the human brain (Guo et al., 2017).

Tau is involved in many different types of dementia, classified as tauopathies, which include Alzheimer's disease (AD), corticobasal degeneration, frontotemporal dementia and progressive supranuclear palsy (Quinn et al., 2018), all of which share the hallmark formation of intraneuronal neurofibrillary tangles. In these diseases, tau is subjected to many post-translational modifications such as phosphorylation, acetylation or proteolysis. These modifications can exacerbate tau aggregation as neurofibrillary tangles, but also induce a toxic gain-of-function of tau as monomers or oligomers (de Calignon et al., 2010; Patterson et al., 2011; Takeda et al., 2015; Ozcelik et al., 2016; d'Orange et al., 2018; Quinn et al.,

*Corresponding authors.
E-mail addresses: anne.fourest-lieuvin@univ-grenoble-alpes.fr (A. Fourest-Lieuvin), isabelle.arnal@univ-grenoble-alpes.fr (I. Arnal).
† Present address: Université Sorbonne, Faculté de Médecine Pitié-Salpêtrière, 75013 Paris, France.

Abbreviations: AD, Alzheimer's disease; CTEV, C-terminal half of the TEV protease; CTRL, control condition; CUT, cleavage condition; FKBP, FK506-binding protein; FRB, FKBP-rapamycin binding domain of mTOR kinase; GFP or EGFP, enhanced Green fluorescent Protein; mCh, mCherry fluorescent protein; MEF, Mouse Embryonic Fibroblast; MTT, Methylthiazolyldiphenyl-tetrazolium bromide; NTEV, N-terminal half of the TEV protease; SDS-PAGE, sodium dodecyl sulfate–polyacrylamide gel electrophoresis; tau-TEV, tau protein with TEV recognition motif; TEV, Tobacco Etch Virus.

https://doi.org/10.1016/j.neuroscience.2022.08.016
0306-4522/

2018; Martinisi et al., 2021). Indeed, recent studies have shown that soluble pathological variants of tau can still interact with microtubules to modulate their organization (Afreen et al., 2017; Prezel et al., 2018; Afreen and Ferreira, 2019; Sohn et al., 2019). Moreover, impaired organization of the actin cytoskeleton has also been reported in AD and in several models of tauopathies (Frandemiche et al., 2014; Zempel et al., 2017; Zhou et al., 2017; Afreen and Ferreira, 2019). Although cytoskeleton defects have always been thought to be involved in disease progression, there is still no clear picture of how abnormal forms of tau affect the cytoskeleton and alter neuronal architecture.

In a disease context, tau cleavage has been identified at various sites. Indeed, tau is a substrate for apoptotic proteases, including caspases 2, 3 and 6, as well as for other proteases like calpains 1 and 2, thrombin, cathepsins, and asparagine endopeptidase (Fasulo et al., 2000; Gamblin et al., 2003; Fasulo et al., 2005; Park and Ferreira, 2005; Zhang et al., 2014; Matsumoto et al., 2015; Zhao et al., 2016; Novak et al., 2018; Quinn et al., 2018). Furthermore, many fragments produced by unidentified proteases have been purified from AD brain tissues (Zilka et al., 2006; Wray et al., 2008; Derisbourg et al., 2015). Overall, up to 50 different proteolytic tau fragments have been proposed to play a role in the pathogenesis of tauopathies (Quinn et al., 2018). Proteolysis can destabilize the primary structure of tau, thereby preventing it from folding correctly into its paper-clip-like tertiary structure (Novak et al., 2018). Misfolding then leads to misregulation of the cytoskeleton-binding domain of tau, with some N- and C-terminally truncated tau proteins exerting 3–4 times higher microtubule assembly activity than full-length tau, to produce abnormally thick microtubule bundles (Zilka et al., 2006; Derisbourg et al., 2015; Prezel et al., 2018).

To study tau truncation and toxicity, research groups have classically expressed truncated fragments in cells (Fasulo et al., 2005; Zilka et al., 2006; Paholikova et al., 2015; Bondulich et al., 2016; Torres-Cruz et al., 2016; Zhao et al., 2016; Afreen and Ferreira, 2019; Guo et al., 2019). However, a single cleavage event at a unique site produces both N- and C-terminal fragments, which might both contribute to perturbing the cell physiology by different mechanisms. To reproduce tau cleavage in cells, we adapted the inducible TEV (Tobacco Etch Virus) protease system (Wehr et al., 2006; Gray et al., 2010), using it to specifically cleave engineered tau proteins at chosen sites. For this study, we used the TEV system to concomitantly apprehend the fate of the N- and C-terminal tau fragments released in the cell and, in particular, to examine their relationship with the cell cytoskeleton. We chose to cleave tau at positions selected as they are known to be cleaved in AD: positions 124 (cleaved by an unknown protease, Derisbourg et al., 2015), 256 and 369 (both of which are cleaved by an asparagine endopeptidase, Zhang et al., 2014), and 392 (also cleaved by an unknown protease, Zilka et al., 2006). In addition, we generated a TEV site at position 198, which is located between tau's two proline-rich domains, P1 and P2. Cleavage at this position produced the following two synthetic fragments: an N-terminal fragment corresponding to the whole projection domain, and a C-terminal fragment encompassing the cytoskeleton-binding domain of tau. This C-terminal fragment was initially called the "assembly fragment" as it contains all the sequences required for both actin and microtubule binding (Brandt and Lee, 1993; Preuss et al., 1997; He et al., 2009; Elie et al., 2015; Prezel et al., 2018).

Our results show that the TEV system cleaves engineered tau proteins in various model cells, yielding N- and C-terminal fragments of the expected sizes. Cleavage at some sites induced cell toxicity, which may be due to altered localizations of tau fragments. Indeed, compared to full-length tau – which localizes to both microtubules and actin filaments – the fragments showed a preference for one or the other cytoskeleton, or were diffuse in the cytosol. Furthermore, some N-terminal fragments relocalized to the nucleus. The TEV system thus appears to be a valuable tool to reproduce specific tau cleavage events in cells and examine the consequences of the simultaneous presence of N- and C-terminal fragments.

EXPERIMENTAL PROCEDURES

Plasmid DNA and lentiviruses

Plasmids used in this study are available on request. All tau constructs were based on the human tau isoform with one N-terminal insertion (N1) and four cytoskeleton-binding repeat (R) motifs (tau-1N4R, 412 amino-acids, NCBI reference sequence NP_001116539.1) and were cloned in the pSIN-EF1alpha lentiviral vector. This vector was produced from the pSIN-W-PGK-GDNF plasmid (Deglon et al., 2000), by replacing the PGK-promoter-GDNF sequence with the EF1alpha-promoter sequence (Table 1). For the GFP-tau construct, EGFP-tau-1N4R was PCR-amplified from the pEGFP-tau-1N4R plasmid (described in Ramirez-Rios et al., 2016) before sub-cloning into the pSIN-EF1alpha vector using the In-Fusion HD Cloning kit (Clontech, #639650). For the GFP-tau-mCh construct, PCR-amplified EGFP-tau-1N4R was sub-cloned into the pmCherry-N1 plasmid (Clontech, #632523). The whole EGFP-tau 1N4R-mCherry sequence was then sub-cloned into the pSIN-EF1alpha vector. For the various tau-TEV constructs, the TEV recognition motif was inserted into the tau sequence contained in the GFP-tau-mCh plasmid at specific locations using the In-Fusion HD Cloning kit. Insertion positions are indicated in Table 1.

To produce GFP-124N, GFP-124C, GFP-256N and GFP-256C constructs, the EGFP sequence was cloned in the pSIN-EF1alpha vector, and then fragments of the tau-1N4R sequence were PCR-amplified and sub-cloned in the NdeI site downstream EGFP (Table 1).

Cleavage of the tau-TEV proteins in cells was induced using an adaptation of the TEV system used in (Gray et al., 2010) in the Lenti-X™ iDimerize™ Inducible Heterodimer System (Clontech, #635075). For this system, the N-terminal half of the TEV protease (NTEV) was PCR-amplified from the pQCXIP-FRB-NTEV plasmid and cloned downstream of the DmrC sequence in the pLVX-Het-1 vector; similarly, the C-terminal half of the

Please cite this article in press as: Fourest-Lieuvin A et al. Controlled Tau Cleavage in Cells Reveals Abnormal Localizations of Tau Fragments. Neuroscience (2022), https://doi.org/10.1016/j.neuroscience.2022.08.016

Table 1. Description of constructs used.

Construct name	description	Map file
NTEV	N-terminal half of the TEV sequence (residues 1–118) cloned in pLVX-Het-1 lentiviral vector	N-TEV in pLVX-Het-1.gb
CTEV	C-terminal half of the TEV sequence (residues 119–242) cloned in pLVX-Het-2 lentiviral vector	C-TEV in pLVX-Het-2.gb
pSIN-EF1alpha lentiviral vector	Plasmid pSIN-W-PGK-GDNF (Deglon et al., 2000) in which PGK-GDNF sequence was replaced by the EF1alpha promoter	pSIN-EF1alpha.gb
GFP-tau	EGFP-tau-1N4R cloned in the pSIN-EF1alpha vector	GFP-tau.gb
GFP-tau-mCh	EGFP-tau-1N4R-mCherry cloned in the pSIN-EF1alpha vector	GFP-tau-mCh.gb
tau-TEV124	TEV motif inserted between T123 and Q124 in the tau sequence of GFP-tau-mCh	tau-TEV124.gb
tau-TEV198	TEV motif inserted between Y197 and S198 in the tau sequence of GFP-tau-mCh	tau-TEV198.gb
tau-TEV256	TEV motif inserted between N255 and V256 in the tau sequence of GFP-tau-mCh	tau-TEV256.gb
tau-TEV369	TEV motif inserted between N368 and K369 in the tau sequence of GFP-tau-mCh	tau-TEV369.gb
tau-TEV392	TEV motif inserted between E391 and I392 in the tau sequence of GFP-tau-mCh	tau-TEV392.gb
pSIN-EF1alpha-EGFP lentiviral vector	Plasmid pSIN-EF1alpha where EGFP sequence was inserted in the SalI site downstream of the EF1alpha promoter	pSIN-EF1alpha-EGFP.gb
GFP-124N	Residues 2–123 of tau-1N4R cloned in NdeI site downstream of EGFP in pSIN-EF1alpha-EGFP vector	GFP-124N.gb
GFP-124C	Residues 124–441 of tau-1N4R cloned in NdeI site downstream of EGFP in the pSIN-EF1alpha-EGFP vector	GFP-124C.gb
GFP-256N	Residues 2–255 of tau-1N4R cloned in NdeI site downstream of EGFP in the pSIN-EF1alpha-EGFP vector	GFP-256N.gb
GFP-256C	Residues 256–441 of tau-1N4R cloned in NdeI site downstream of EGFP in the pSIN-EF1alpha-EGFP vector	GFP-256C.gb

All plasmids and map files are available on request.

TEV protease was PCR-amplified from the pQCXIH-FKBP-CTEV and cloned downstream of the DmrA sequence in the pLVX-Het-2 vector.

For lentiviral production and cell transfection, plasmid DNA was prepared using a Nucleobond Xtra Midi Endofree Kit (Macherey-Nagel, #740420.50). Lentiviral particles were produced in our virus production facility by co-transfection of each plasmid described above with the psPAX2 and pCMV-VSV-G helper plasmids (Addgene) into HEK293T cells obtained from ATCC (ATCC-CRL-3216). Viral particles were collected by ultra-speed centrifugation and titrated by serial dilution and immunofluorescence observation of transduced COS-7 cells. Stock aliquots of lentiviruses were prepared at a titer of 50×10^6 IU/mL, and stored at −80 °C until use.

Cell culture, transfections, transductions and treatments

Mouse Embryonic Fibroblasts (MEF) were obtained as described (Tan and Lei, 2019) from dissected mesenchymal tissues from wild-type Swiss/CD1 mouse (Janvier Labs, #SN-SWISSF) embryos at E14.5. MEF, COS-7 and HeLa cells were cultured in DMEM 4.5 g/L glucose (ThermoFisher scientific, #31966047) supplemented with 10% fetal bovine serum (ThermoFisher scientific, #10270106) and 1 × penicillin–streptomycin (ThermoFisher scientific, # 15140122) at 37 °C and 5% CO_2 in a humidified incubator.

On the day before transfection or transduction, cells were plated in 35-mm dishes or 24-well plates. Transient transfections were performed with 1 μg of plasmid DNA per 35-mm dish, using the Lipofectamine 3000 reagent (ThermoFisher scientific, #L3000008). After transfection, cells were incubated for 24–36 h before observation by immunofluorescence.

For viral transduction experiments, the aliquots of stock lentiviruses were thawed just before use and diluted tenfold in culture medium at room temperature, to produce working solutions at 5×10^6 IU/mL. For control conditions (CTRL conditions), cells in 35-mm dishes were transduced with 25 μL of one tau-TEV virus and 20 μL of the NTEV virus (volumes indicated correspond to working solutions). For cleavage conditions (CUT conditions), cells were transduced with 25 μL of one tau-TEV virus together with 10 μL of NTEV virus and 10 μL of CTEV virus. The day after transduction, cells were treated twice with 25 nM rapalog (or A/C heterodimerizer, Clontech, #635057), with 8–9 h between the two treatments. The next day, cells were processed for western blotting, immunofluorescence, or MTT assays. In summary, experiments involved four steps performed at one-day intervals: day 1, cell seeding; day 2, transduction; day 3, rapalog treatment; day 4, cell processing for analysis (see below).

MTT cell viability assay

MTT (Methylthiazolyldiphenyl-tetrazolium bromide, Sigma-Aldrich, #M2128) is a yellow tetrazole which is metabolized by mitochondrial dehydrogenases in live cells to produce insoluble purple formazan (Cook and Mitchell, 1989), it is commonly used to assess cell viability. For viability assays, cells were seeded in 24-well plates, transduced with the different lentiviruses and/or treated with rapalog and Taxol, as specified, before incubation with 0.25 mg/mL MTT (final concentration) in culture medium for two hours at 37 °C. The culture

medium was then removed and cells were washed with PBS before adding 200 μL dimethyl sulfoxide to solubilize the formazan crystals. Absorbance was measured at 540 nm and 650 nm (background) using a PHERAstar® FS microplate reader (BMG Labtech). The difference (A_{540}-A_{650}) was calculated. Each condition was tested in triplicate (3 wells).

For negative or positive controls of cell viability, cells were either left untreated (100 % viability) or treated with 100 nM Taxol (Sigma-Aldrich, #T7402) for 24 h before performing the MTT test.

Cell extracts and western blotting

To prepare total cell extracts, cells in 35-mm dishes were treated for 30 sec with 120 μL of lysis buffer (1% SDS in water, with 400 μM phenylmethylsulfonyl fluoride, PMSF, # P7626, Sigma-Aldrich), scraped and then sonicated for 30 sec on ice. To produce Triton-soluble and insoluble cell fractions, cells in 35-mm dishes were washed once with 1 mL serum-free DMEM at 37 °C, then extracted for 1 min at 37 °C with 120 μL of OPT buffer (80 mM Pipes, pH 6.7, 1 mM EGTA, 1 mM $MgCl_2$, 0.5% Triton X-100, 10% glycerol, and supplemented with 400 μM PMSF). This first extract – the soluble fraction – was kept on ice before SDS-PAGE. Cells were then washed with 1 mL OPT buffer at 37 °C, and were incubated into 120 μL of lysis buffer for 30 sec, then scraped and sonicated for 30 sec on ice to produce the insoluble fraction. After addition of Laemmli buffer, equal volumes of total extracts, soluble and insoluble fractions, were loaded onto acrylamide gels.

SDS-PAGE and western blotting were performed according to standard procedures. Primary antibodies used on blots were a rat monoclonal antibody directed against EGFP (Chromotek, #3H9), a rabbit polyclonal antibody against mCherry (Rockland, #600-401-379) and a rabbit polyclonal antibody against actin (Sigma-Aldrich, #A2066). Horseradish peroxidase-conjugated secondary antibodies were purchased from ThermoFisher scientific. Blots were revealed using SuperSignal™ West Pico PLUS Chemiluminescent Substrate (ThermoFisher scientific, #34577). Images were acquired on a ChemiDoc-MP Gel Imaging System (BIO-RAD laboratories).

Immunofluorescence and image acquisition

To fix cells, cell culture medium was removed and cells on coverslips were treated for 10 min at 37 °C in a solution of 0.5% glutaraldehyde, 0.1% Triton X-100, 10% sucrose in "cytoskeleton buffer" (CB, 10 mM MES, 138 mM KCl, 3 mM $MgCl_2$, 2 mM EGTA, pH = 6.1). Cells were then rinsed in CB at room temperature and glutaraldehyde auto-fluorescence was quenched for 10 min with 1 mg/mL $NaBH_4$ in PBS. After quenching, cells were rinsed twice with PBS and then saturated for 30 min in PBS containing 0.1% Tween 20. All reagents for fixation were from Sigma-Aldrich, except glutaraldehyde (Electron Microscopy Sciences, #16220). Immunofluorescence was then performed using standard procedures. Primary antibodies were a rabbit polyclonal antibody directed against EGFP (Millipore, #AB3080) and a monoclonal antibody directed against alpha-tubulin (α3-a1, Peris et al., 2006). Secondary antibodies were coupled to Alexa-488, Alexa-647, or Cyanine3 (Jackson Immuno-Research Laboratories). Actin was stained with 50 nM Atto647-phalloidin or Atto565-phalloidin (Atto-Tec GmbH, #AD647-81 or #AD565-81) during the incubation with secondary antibodies. DNA was stained with 5 μg/mL bisBenzimide Hoechst 33258 (Sigma-Aldrich, #14530). Images were acquired on a Zeiss LSM 710 confocal microscope equipped with a Zeiss AiryScan module, using a 63x oil-immersion NA 1.4 objective and Zen software (Carl Zeiss MicroImaging).

Quantifications and statistics

To evaluate the number of cells with a green stained nucleus, HeLa and COS-7 cells were examined and counted on single plane confocal airyscan images. MEF cells were examined and counted directly under the fluorescence microscope as their large size was incompatible with counting of multiple cells on a single image. In this case, cells were counted on several distinct coverslips for each experiment (see legend to Fig. 4).

The localizations of tau-TEV proteins (in CTRL and CUT conditions), GFP-tau full-length protein, and GFP-tau fragments with respect to the cytoskeleton were examined both directly under the fluorescence microscope (according to the localization patterns described in Fig. S1) and by quantification on single plane confocal airyscan images as described below.

An ImageJ macro was used to quantify colocalization of the various tau proteins with actin, microtubules, and cytosolic compartments. Briefly, for each cell a cytoplasmic region was selected excluding the perinuclear region. Actin and microtubule channels in this region were denoised using the A-Trou filter (https://imagej.nih.gov/ij/plugins/a-trous-wavelet-filter.html). Images were then thresholded to produce masks on the cytoskeleton fibers. These masks were combined by subtracting them from the GFP channel (or mCherry channel) to produce actin-only, microtubule-only, and free cytosol (neither on actin nor on microtubules) compartments. Mean GFP intensities (or mean mCherry intensities) were measured in the whole region (GFPtotal), on actin fibers (GFPactin), on microtubules (GFPmt), and in the free cytosolic compartment (GFPcyto). Ratios of (GFPactin/GFPtotal), (GFPmt/GFPtotal) and (GFPcyto/GFPtotal) were calculated and expressed as percentages.

All statistical analyses were performed using Prism 6 (GraphPad software, USA). Tests were as specified in figure legends.

RESULTS

Engineering TEV protease and tau to allow site-specific, timed control of tau cleavage

To reproduce the cleavage of full-length tau occurring in cells, we took advantage of the TEV protease. The TEV

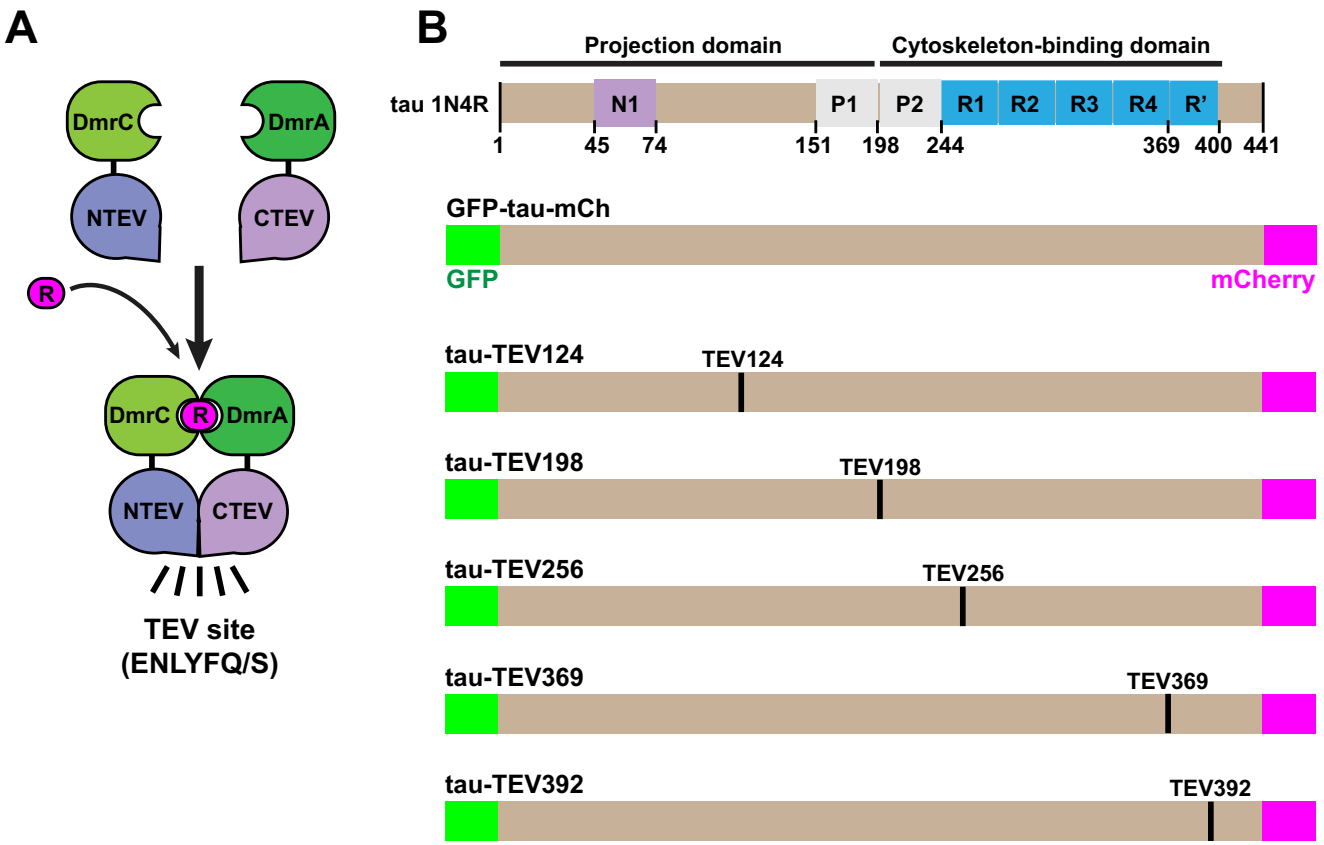

Fig. 1. Description of the TEV system used to induce time- and site-specific truncation of tau. (A) Schematic representation of the TEV system used in this study (adapted from Wehr et al., 2006). The TEV protease is active when DmrA and DmrC peptides dimerize following exposure to rapalog (R). The active protease subsequently cleaves TEV sites (amino acid sequence ENLYFQ/S where "/" is the site of cleavage). DmrA-CTEV (named CTEV) and DmrC-NTEV (named NTEV) were produced in lentiviral vectors. **(B)** Schematic representation of the tau 1N4R isoform, and constructs used in this study. N1 is an N-terminal insert, P1 and P2 are proline-rich sequences, R1 to R4 are repeat sequences, and R′ is a pseudo-repeat motif. The projection domain comprises the N-terminal part of tau including N1 and P1 sequences, and the cytoskeleton-binding domain comprises the P2 motif and R1 to R′ sequences. By convention, the numbering corresponds to the amino-acid positions in the longest tau isoform (2N4R), even though all constructs were based on the tau 1N4R isoform. For tau-TEV constructs, the locations of each inserted TEV site in the sequence of GFP-tau-mCh are shown. As for NTEV and CTEV, all tau-TEV constructs were packaged in lentiviral vectors.

protease specifically cleaves proteins containing a seven-amino-acid sequence (ENLYFQ/S), which is not naturally present in the mammalian proteome and can therefore be introduced to create engineered target proteins. To use the TEV protease in an inducible manner, we adapted the system developed by Wehr et al. (2006) and optimized by Gray et al. (2010), where the N- and C-terminal parts of the protease are fused to FRB (the FKBP-rapamycin binding domain of mTOR kinase) and FKBP, respectively. With these constructs, TEV protease activity is only activated following the addition of rapamycin or rapamycin analogs, which trigger FRB and FKBP dimerization. We cloned the TEV system in the Lenti-X iDimerize Inducible Heterodimer System (Clontech). The N-terminal half of TEV was fused to the DmrC peptide (corresponding to the mutated FRB described in Gray et al., 2010) and the C-terminal half of TEV was fused to the DmrA peptide (or FKBP peptide) (Fig. 1A). Both constructs were packaged in distinct lentivirus vectors. Lentiviruses expressing DmrC-NTEV and DmrA-CTEV were used to transduce cells. Rapalog (or A/C heterodimerizer, Clontech) was subsequently added to the cell culture medium to induce rapid heterodimerization of the DmrC and DmrA peptides and thus trigger activation of the TEV protease (Fig. 1A). For simplicity, DmrC-NTEV and DmrA-CTEV lentiviruses are hereafter referred to as NTEV and CTEV viruses.

In addition to the TEV protease, we generated a full-length tau construct (1N4R isoform) with an EGFP moiety (called GFP hereafter) at its N-terminus and an mCherry (or mCh) at its C-terminus (GFP-tau-mCh construct, Fig. 1B). From this construct, we produced several related constructs by inserting a TEV recognition cleavage motif at positions 124, 198, 256, 369, and 392 (Fig. 1B). Most of these positions were selected as they are known to be cleaved in AD (see introduction). The GFP-tau-mCh constructs with inserted TEV motifs are hereafter referred to as tau-TEVs.

Tau-TEV proteins are effectively cleaved by the inducible TEV system

We first tested the various tau-TEV constructs in transfection experiments with MEF cells – primary fibroblasts with well-defined microtubule and actin arrays – and compared their expression patterns to

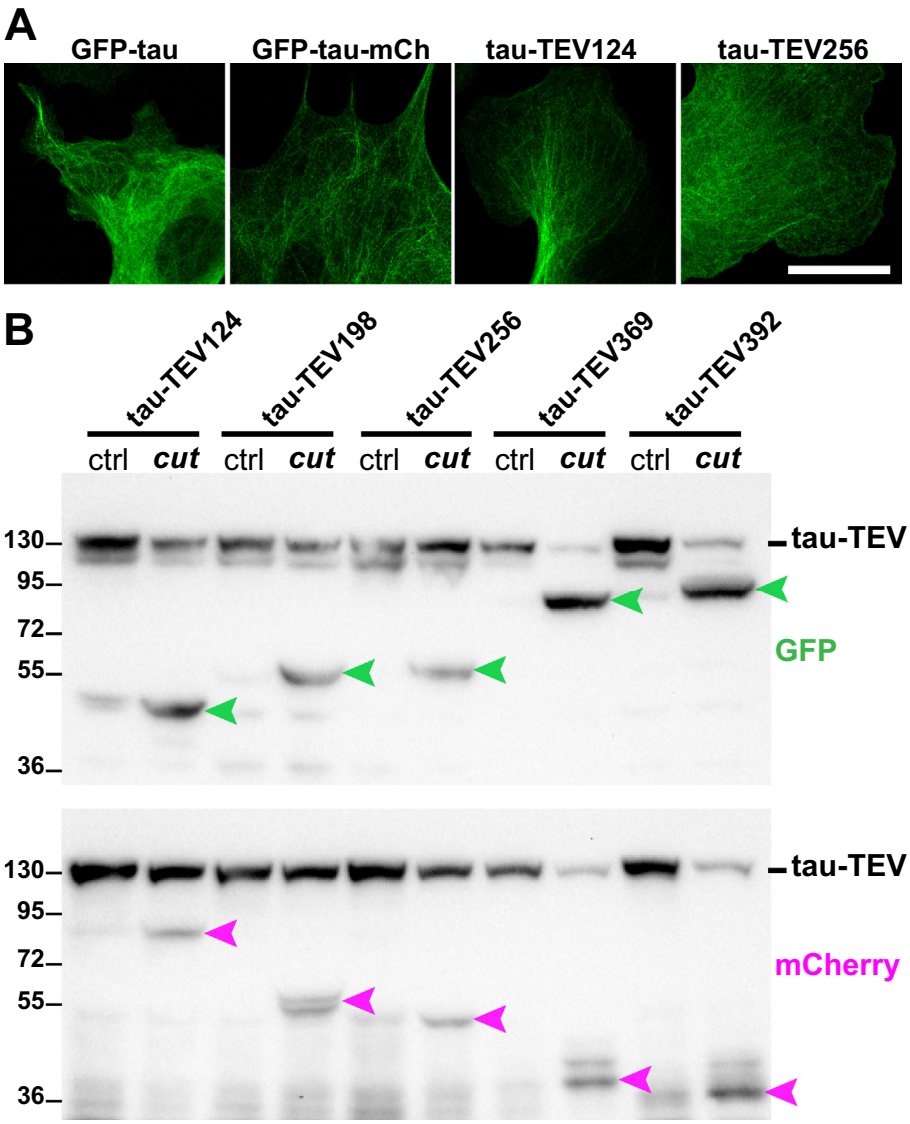

Figure 2

Fig. 2. Validation of the TEV system applied to tau protein. (**A**) MEF cells transfected with plasmids encoding GFP-tau, GFP-tau-mCh, and Tau-TEVs (tau-TEV124 and tau-TEV256 are shown) and stained with an anti-GFP antibody. The tau-TEV constructs expressed exhibit a filamentous pattern similar to that observed with control tau constructs (GFP-tau and GFP-tau-mCh). Scale bar = 20 μm. **(B)** COS-7 cells were transduced with one tau-TEV lentivirus together with the NTEV virus alone (control condition, CTRL), or with both the NTEV and CTEV viruses (cleavage condition, CUT). All cells (CTRL and CUT conditions) were treated with rapalog 24 h before protein extraction and western blotting. Western blots were revealed using anti-GFP (top) and anti-mCherry (bottom) antibodies. Western blots reveal the presence of GFP N-terminal fragments (green arrowheads) and mCherry C-terminal fragments (magenta arrowheads) for all tau-TEV proteins in CUT conditions. Tau-TEV proteins and fragments were of the expected sizes. Molecular weights (in kDa) are shown to the left of each blot.

those of unmodified GFP-tau and GFP-tau-mCh constructs (Fig. 2A). Cells expressing the tau-TEV proteins exhibited the same filamentous staining pattern as GFP-tau and GFP-tau-mCh (Fig. 2A). This pattern is typical of either microtubules or actin filaments (see Fig. S1), thus indicating that insertion of the seven-amino-acid TEV motif into the tau sequence had no effect on its overall localization in cells. The various tau-TEV constructs were then packaged in lentiviruses for the experiments described below.

We next examined whether both GFP and mCherry tau fragments could be detected after cleavage of tau-TEVs, induced by activation of the TEV protease in cells. COS-7 cells were transduced with each tau-TEV lentivirus, together with either the NTEV virus alone (control condition, CTRL), or with both the NTEV and CTEV viruses (cleavage condition, CUT). All cells (CTRL and CUT conditions) were treated with rapalog before protein extraction and western blotting. Results showed the production of both GFP-N-terminal and C-terminal-mCherry tau fragments of the expected sizes in the CUT conditions (Fig. 2B and Table 2). Cleavage of tau-TEV369 and tau-TEV392 was nearly complete, whereas a large amount of non-cleaved tau-TEV124, tau-TEV198 and tau-TEV256 subsisted, suggesting that cleavage was more efficient at some sites than others.

In conclusion, the adapted TEV system can effectively be used to induce time- and site- specific cleavage of tau in model cells. Furthermore, fragment species are produced alongside a certain amount of the full-length tau, which is reminiscent of the pathological situation in AD neurons.

Cleavage at specific sites of tau is toxic for cells

We next wondered if the presence of tau fragments in cells impaired cell viability, as expected for fragments identified in a pathological context. Cell toxicity was tested using the MTT viability assay. We first checked that rapalog was not toxic for MEF cells in our working conditions (Fig. 3A). Cell viability was then examined for each tau-TEV in both CTRL and CUT conditions. Results showed that cleavage of tau-TEV198 and tau-TEV369 had no effect on cell viability, whereas cleavage of tau-TEV124, tau-TEV256, and tau-TEV392 was toxic for cells (Fig. 3B). Hence, the cleavage of tau at some specific sites is deleterious for cells.

Please cite this article in press as: Fourest-Lieuvin A et al. Controlled Tau Cleavage in Cells Reveals Abnormal Localizations of Tau Fragments. Neuroscience (2022), https://doi.org/10.1016/j.neuroscience.2022.08.016

Table 2. Calculated sizes of tau fragments *vs* their apparent size on SDS-PAGE gels.

Name of tau-TEV	Tau-TEV fragment	Theoretical size (kDa)	Apparent size on gel (kDa)
All tau-TEV	Non-cleaved	101	130
Tau-TEV124	GFP-N-terminal	37	50
	C-terminal-mCherry	61	80
Tau-TEV198	GFP-N-terminal	45	55
	C-terminal-mCherry	56	55
Tau-TEV256	GFP-N-terminal	55	60
	C-terminal-mCherry	49	50
Tau-TEV369	GFP-N-terminal	64	80
	C-terminal-mCherry	37	40
Tau-TEV392	GFP-N-terminal	67	90
	C-terminal-mCherry	35	38

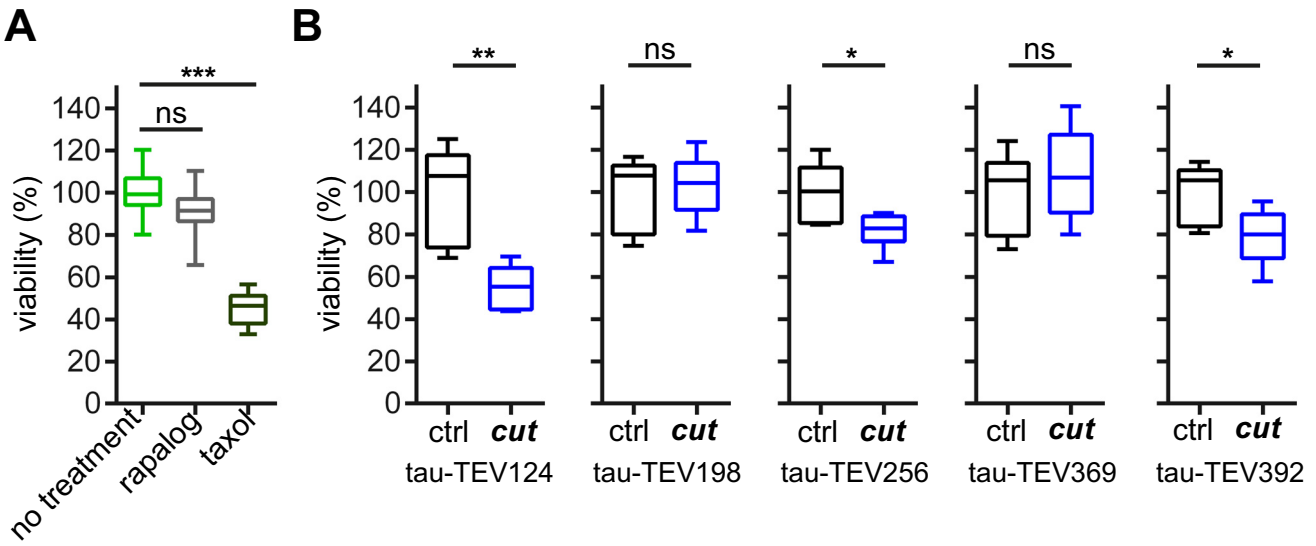

Fig. 3. Impact of tau cleavage on cell viability. (A) MTT viability tests show that the rapalog treatment used to activate the TEV protease is not toxic for cells, unlike Taxol, which was used here as a positive control. Number of tests from two independent experiments: no treatment, 18; rapalog, 18; Taxol, 11. ns, non-significant, ***$P < 0.001$, Kruskal-Wallis test with Dunn's multiple comparisons. **(B)** MTT viability tests performed for each tau-TEV construct in CTRL and CUT conditions. Results were normalized by expressing them as percentages of the mean in CTRL condition for each tau-TEV. They show a significant decline in cell viability after cleavage of tau-TEV124, tau-TEV256 and tau-TEV392. For each tau-TEV in CTRL and CUT condition, six tests from two independent experiments were performed. ns, non-significant, *$P < 0.05$, **$P < 0.01$. Mann-Whitney tests.

N-terminal fragments released from tau cleavage at sites 124 or 256 relocalize to the nucleus

Based on the results presented above, we decided to focus on tau cleavage at positions 124 and 256, since the fragments released have a toxic effect on cells. We used immunofluorescence to examine how the fragments behaved following activation of the TEV protease in transduced MEF cells. In CTRL conditions with the tau-TEV124 and tau-TEV256 proteins, GFP and mCherry staining overlapped as expected (Fig. 4A, B, upper panels). In CUT conditions, the nucleus was stained green in many cells transduced with tau-TEV124 or tau-TEV256, as a consequence of nuclear relocalization of GFP N-terminal fragments (Fig. 4A, B, bottom panels). Quantification indicated that nuclear relocalization of GFP N-terminal fragments occurred in CUT conditions in 82% of cells transduced with tau-TEV124, and in 67.5% of cells transduced with tau-TEV256 (Fig. 4C). Nuclear relocalization of N-terminal tau fragments after rapalog-induced activation of the TEV protease was also observed in COS-7 and HeLa cells (Fig. S2A, B), but to a lesser extent than in MEF cells (Fig. S2C, D). This difference might be due to variable cleavage efficiency between cell types.

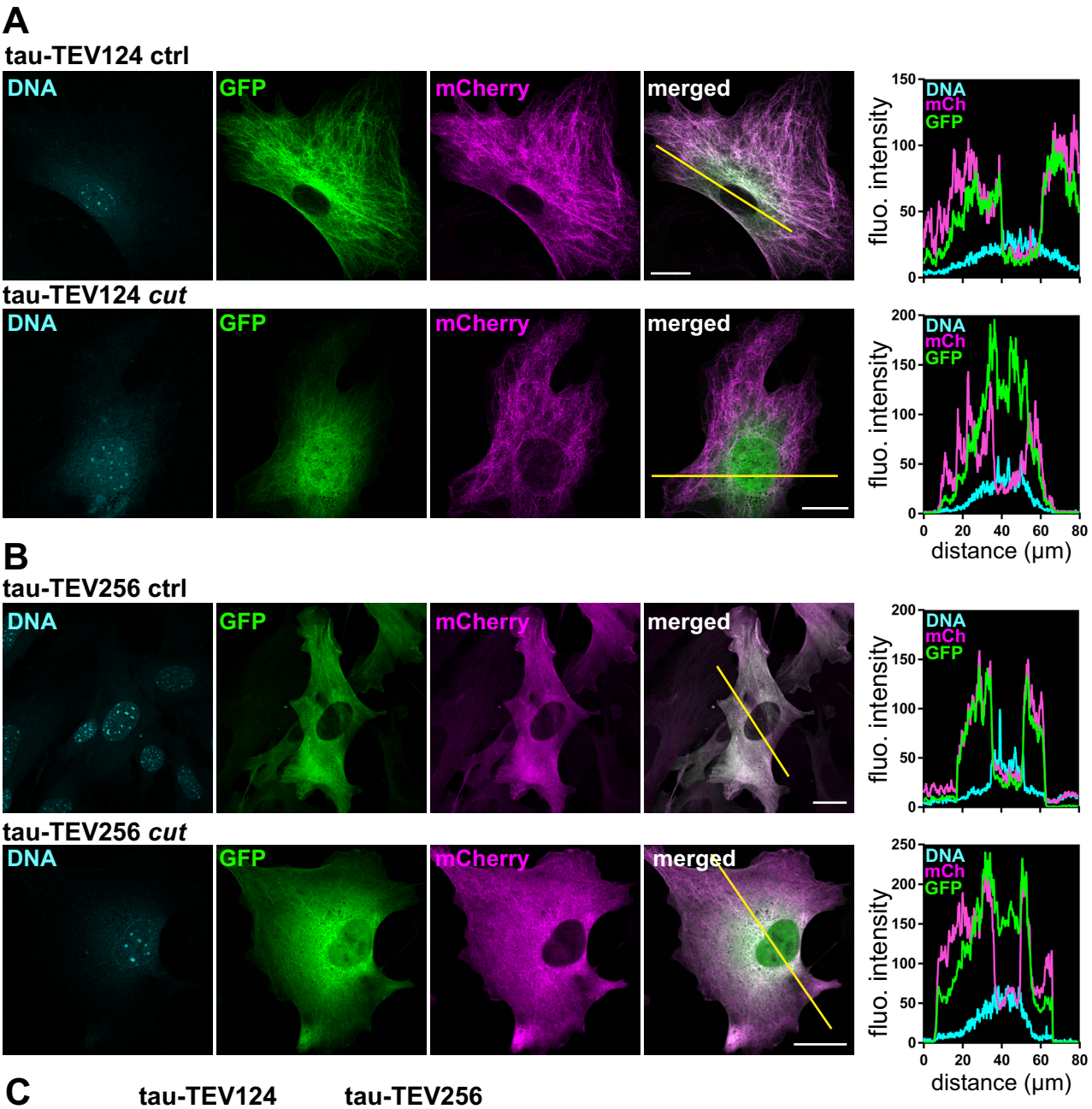
A
tau-TEV124 ctrl
DNA
GFP
mCherry
merged
DNA
mCh
GFP
fluo. intensity
tau-TEV124 cut
B
tau-TEV256 ctrl
tau-TEV256 cut
distance (µm)
C
tau-TEV124
tau-TEV256
green nuclei
(% of transduced cells)
**
(0%)
ctrl
cut

Cytoskeleton localization of tau fragments following TEV cleavage

The main function of tau is to bind and regulate both the microtubule and actin cytoskeletons (Kanai et al., 1992; Fulga et al., 2007; Elie et al., 2015; Biswas and Kalil, 2018; Prezel et al., 2018). Tau cleavage might impair this function, leading to aberrant localizations of fragments on the microtubule and/or actin cytoskeletons. Tau fragment localization was examined in MEF cells. Cells were labeled in CTRL and CUT conditions with antibodies recognizing GFP and mCherry in combination with either anti-alpha-tubulin antibody (microtubules) or phalloidin (actin). In CUT conditions, to ensure that a cleavage event had occurred, only cells with a green nucleus were analyzed. Cells were classified depending on the localization patterns of full-length tau and its fragments in the following four categories: (i) diffuse localization in the cytosol (without cytoskeleton-like pattern), or localization on (ii) microtubules, (iii) actin, or (iv) both cytoskeletons (Fig. S1). It should be noted that, in our experimental conditions, it was impossible to stain both cytoskeletons (microtubules and actin filaments) while also staining the GFP and mCherry fragments. Nonetheless, based on their fluorescence pattern, tau-TEV proteins or fragments could clearly be localized to one or the other cytoskeleton, or both cytoskeletons, even in the absence of specific microtubule or actin labeling.

For tau-TEV124, we observed the non-cleaved protein to exhibit a microtubule-associated pattern in 62% of transduced cells in CTRL conditions (Fig. 5A, D). Tau-TEV124 also localized with actin in 7% of cells, and with both cytoskeletons in 30% of cells (Fig. 5D). In CUT cells, the N- and C-terminal tau fragments released adopted completely different localizations compared to that of non-cleaved tau. The GFP-labeled N-terminal fragment displayed a mostly diffuse staining pattern in the MEF cell cytoplasm (Fig. 5B, C, left panels), and was also observed in the nucleus (Fig. 5B, C, stars) as described above (Fig. 4). In contrast, the mCherry-labeled C-terminal fragment was associated with microtubules in 78% of cells (Fig. 5B, C, "mCherry" panels, arrowheads, quantifications in Fig. 5D), and remained outside the nucleus. Merged images confirmed the distinct localizations of the GFP N-terminal and mCherry C-terminal fragments (Fig. 5B, C).

The phenotype of non-cleaved tau-TEV256 was similar to that of tau-TEV124, with localization on microtubules (Fig. 6A), and on both the actin and microtubule cytoskeletons (Fig. 6B and quantifications Fig. 6E). However, following cleavage at site 256, the fragments showed different localizations compared to the fragments produced by cleavage at site 124. Thus, the two fragments released showed an actin-binding pattern in about 60% of cells, and a diffuse pattern in most of the remaining cells analyzed (Fig. 6C, E). Strikingly, in about 10% of cells, the mCherry C-terminal fragment appeared to localize on microtubules (Fig. 6D, magenta arrowheads), whereas the N-terminal fragment localized on actin stress fibers (Fig. 6D, green arrow). Thus, in these cells, there was a clear segregation of the N- and C-terminal parts of tau between actin and microtubules.

To confirm differences in the localization of tau-TEV proteins before and after cleavage, we analyzed co-localization on confocal airyscan images (Fig. S3, see Experimental Procedures for details). In line with the data presented in Figs. 5 and 6, the results indicated a preferential association of the mCherry C-terminal tau-TEV124 fragment with microtubules, whereas the two tau-TEV256 fragments preferentially associated with actin.

Overall, these results reveal that fragments produced following tau cleavage exhibit novel properties compared to full-length tau. In general, the N-terminal fragment was detected as diffuse staining in the cytosol, with occasional relocalization to the nucleus. In contrast, C-terminal fragments continued to associate with the cytoskeleton, but displayed specific microtubule- or actin-like patterns depending on the specific cleavage sites.

Cytoskeleton localization of individually expressed tau fragments

Tau proteolysis induced using the site-specific TEV system revealed that both N- and C-terminal fragments could exhibit abnormal localizations inside cells, which are likely to affect cell homeostasis. To verify that the observed fragment localizations were not influenced by the type (GFP or mCherry) or position (N- or C-terminal) of the fluorescent label, we generated four constructs corresponding to each fragment with a GFP moiety at their N-terminus, which we named GFP-124N, GFP-124C, GFP-256N and GFP-256C.

The different GFP-tagged fragments packaged in lentiviruses were used to transduce MEF cells, and their

Fig. 4. Relocalization of the N-terminal fragment of tau to the nucleus after cleavage at sites 124 and 256. (A, B) MEF cells expressing tau-TEV124 **(A)** or tau-TEV256 **(B)** in CTRL and CUT conditions. Confocal images of a single focal plane are shown for cells stained with Hoechst 33258 to label DNA (cyan images), and with anti-GFP (green) and anti-mCherry (magenta) antibodies. Merged GFP and mCherry labeling images are shown. Line scan plots (right panels) were produced for each stain, the scan corresponds to fluorescence intensity along the yellow line drawn on the merged images. Plot profiles show that the fluorescence intensity of GFP-tau fragments did not decrease in the nucleus under CUT conditions compared to control conditions. In many cells, the GFP fragment (N-terminal part of tau) of both tau-TEV124 and tau-TEV256 was relocalized to the nucleus in CUT conditions. Scale bars = 20 μm. **(C)** Transduced MEF cells with or without green nuclei were counted to determine the percentage of cells in which the nucleus was stained green in CTRL and CUT conditions. Number of counts performed in two independent experiments: $n = 5$ and 8 counts for tau-TEV124 CTRL and CUT, respectively (276 and 627 cells examined); $n = 5$ and 8 counts for tau-TEV256 CTRL and CUT, respectively (238 and 498 cells). $^{**}P < 0.01$, Mann-Whitney tests.

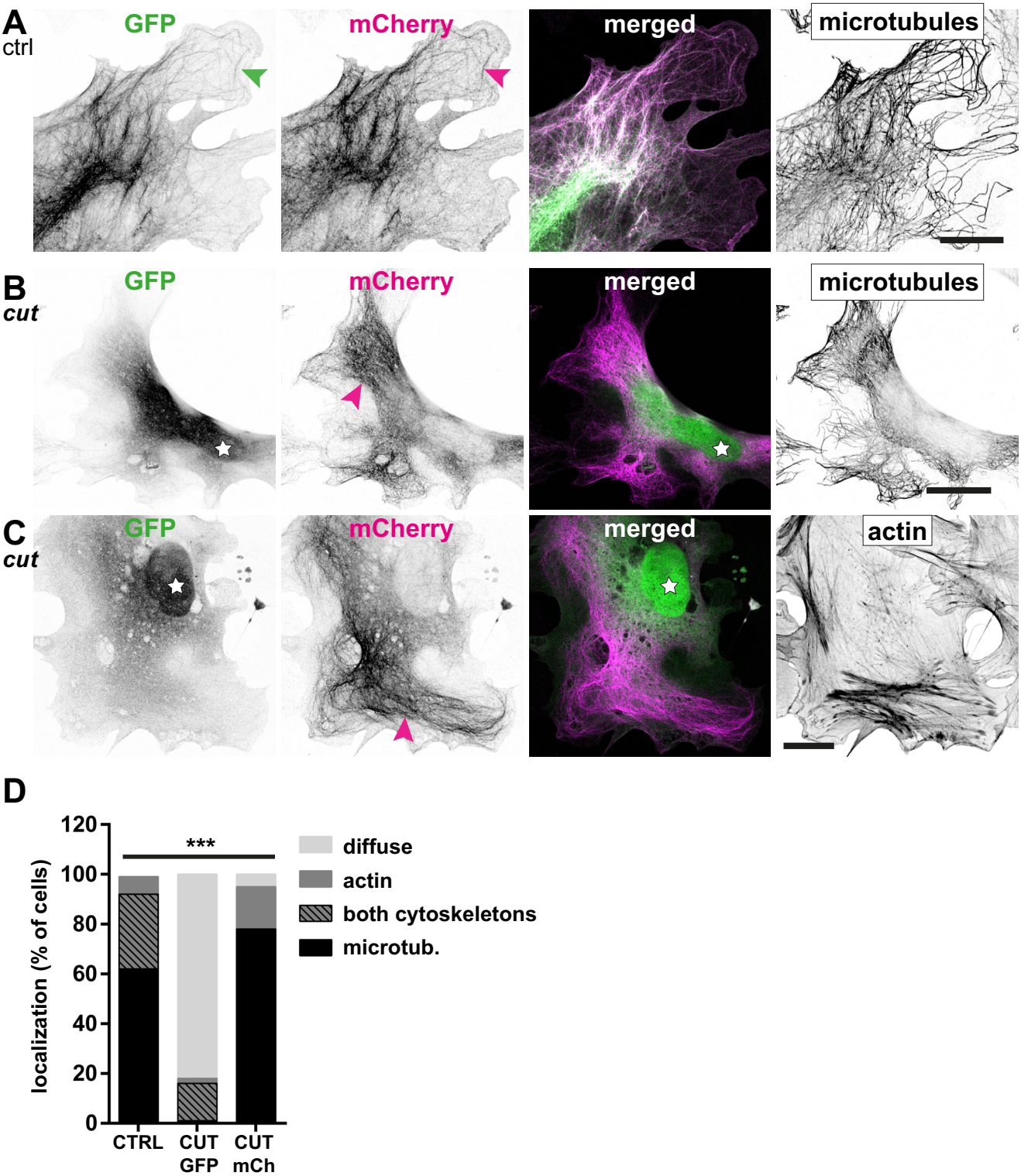

Fig. 5. Relocalization of the N- and C-terminal fragments of tau with regards to the cytoskeleton after cleavage at site 124. (A) In CTRL condition (no cleavage), tau-TEV124 localized mostly on microtubules in transduced MEF cells. **(B, C)** In CUT condition (after cleavage), the GFP N-terminal fragment was mainly cytosolic (diffuse staining), and also entered the nucleus (stars), whereas the mCherry C-terminal fragment remained mostly associated with microtubules (arrowheads). Scale bars = 20 μm. **(D)** Quantification of localization patterns for the non-cleaved tau-TEV124 in control cells (CTRL), or, after cleavage, for the GFP N-terminal fragment (CUT-GFP), or the mCherry C-terminal fragment (CUT-mCh). Cells were distinguished based on the localization patterns of tau or its fragments, as described in Fig. S1: diffuse in the cytosol, localized on actin stress fibers, localized on microtubules, or localized on both cytoskeletons. For the CUT condition, only cells exhibiting a green nucleus were examined since this phenotype was clearly associated with tau cleavage (see Fig. 4). Cells were analyzed in two independent experiments (n = 300 for tau-TEV124 CTRL, n = 245 for CUT-GFP, and n = 129 for CUT-mCh). ***P < 0.001, Chi-square test.

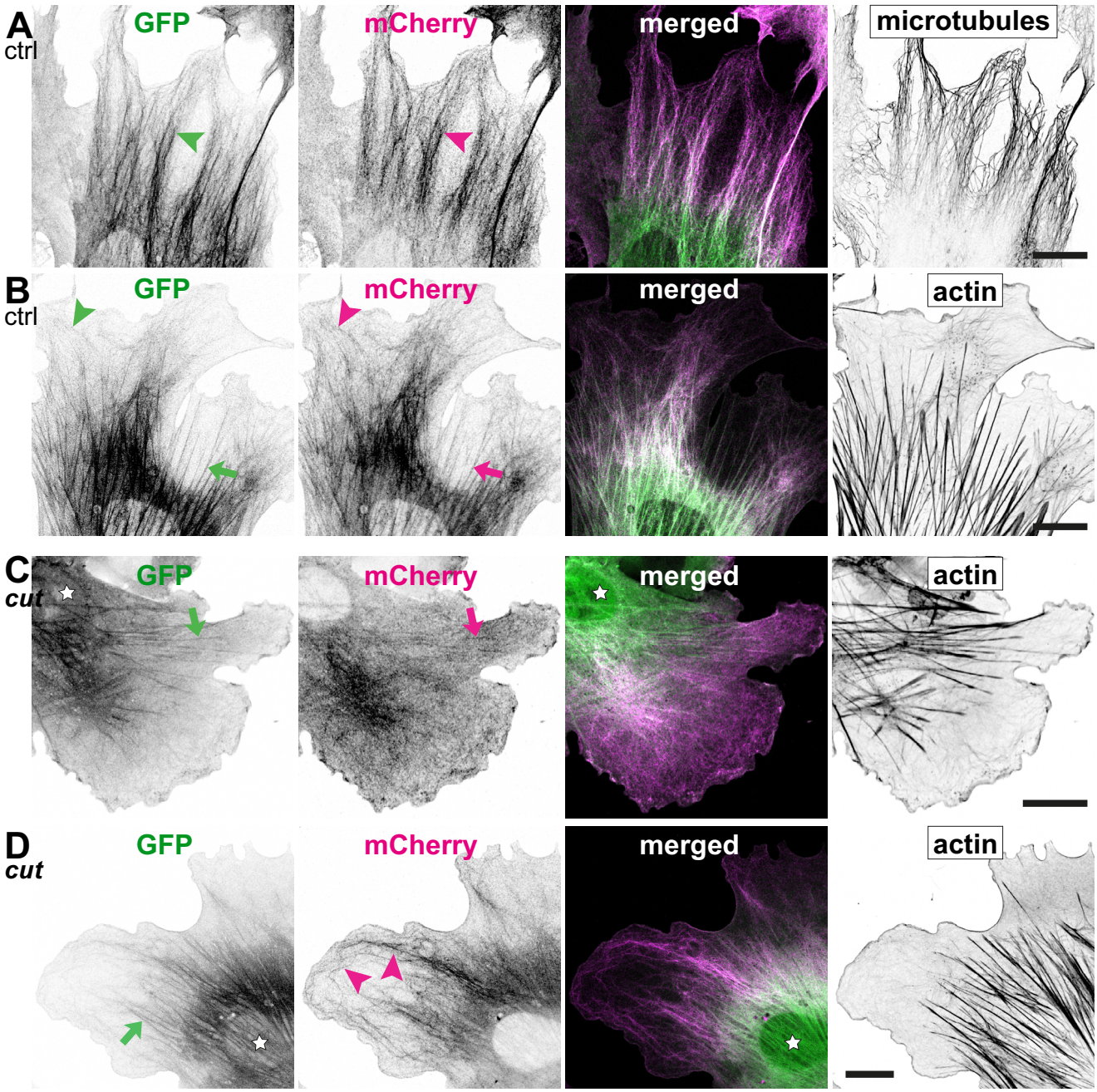
A
ctrl
GFP
mCherry
merged
microtubules
B
ctrl
GFP
mCherry
merged
actin
C
cut
GFP
mCherry
merged
actin
D
cut
GFP
mCherry
merged
actin
E
localization (% of cells)
120
100
80
60
40
20
0
***
CTRL
CUT GFP
CUT mCh
diffuse in cytosol
actin
both cytoskeletons
microtubules

localization patterns were compared to those of full-length GFP-tau 1N4R (GFP-tau, Fig. 7A, first row). In these experiments, microtubules and actin filaments were also labeled (Fig. 7A). As expected, GFP-tau mostly localized on microtubules, actin, or both cytoskeletons (Fig. 7A, first row, and see quantifications Fig. 7B). In contrast, the two N-terminal fragments GFP-124N and GFP-256N were present in the cytoplasm, with a diffuse staining pattern in most cells (Fig. 7A, second and fourth rows, and Fig. 7B). As in the cleavage experiments, in 20% of cells, the GFP-256N fragment co-localized with actin fibers (Fig. 7A, fourth row, arrow). The two C-terminal fragments remained associated with the cytoskeleton, with a preferential localization on microtubules (GFP-124C, Fig. 7A third row) or on actin (GFP-256C, Fig. 7A fifth row). The localization of GFP-124C on microtubules was accompanied by the formation of microtubule bundles (Fig. 7A, third row, green arrowhead), as previously reported (Derisbourg et al., 2015). These results were further confirmed by co-localization studies (Fig. S4A) and western blotting of Triton-soluble/insoluble protein fractions (Fig. S4B). In addition, as expected from the nuclear relocalization of the N-terminal tau-TEV fragments in CUT conditions (Figs. 4 and S2), the GFP-124N and GFP-256N fragments were present in the nuclei of transduced cells (Fig. 7C). Finally, MTT viability tests revealed that, unlike whole cleaved tau-TEV124 and tau-TEV256, the individually expressed fragments were not toxic for cells (Fig. 7D).

In conclusion, although they were less toxic, the different fragments expressed individually exhibited similar localization patterns to those of the tau-TEV fragments released following TEV-induced cleavage.

DISCUSSION

The aim of this study was to determine whether the TEV protease could be used to study tau fragmentation as observed in AD and other tauopathies.

As tau cleavage at one specific site induces the production of two fragments, it was important to be able to study how the simultaneous presence of the two fragments affected cell physiology, in particular the cytoskeleton. Inspired by studies of huntingtin cleavage in the context of Huntington's disease (El-Daher et al., 2015), we developed a tool based on the TEV system (Wehr et al., 2006; Gray et al., 2010) to control tau cleavage in cells in terms of both time and site. The results presented in this article show that the system efficiently induced controlled cleavage of tau at several sites and in several model cells (MEF, COS-7, HeLa cells). Controlled cleavage of tau at positions 124 and 256 resulted in the production of fragments displaying aberrant localizations with respect to the cytoskeleton, and relocalization to the nucleus. These cleavage events were also associated with cell toxicity. Based on the results presented here, the TEV method is a powerful tool to recapitulate the pathological cleavage of tau and decipher the fate and activity of the fragments released in cells.

One striking event linked to tau truncation in our study was the partial relocalization of N-terminal tau fragments to the nucleus (Figs. 4 and S2). Relocalization varied depending on the cleavage site and/or the cell type, possibly due to variable cleavage efficiency (Fig. 2B). Nuclear pore complexes are responsible for protein trafficking between the cytoplasm and the nucleoplasm. Molecules smaller than about 30–60 kDa can migrate freely through these nuclear pore complexes via passive transport (Timney et al., 2016) which might explain the partial nuclear relocalization of the GFP N-terminal fragments produced from tau-TEV124 and tau-TEV256 (theoretical sizes of 37 kDa and 55 kDa, respectively). The N-terminal fragment produced from tau-TEV124 is smaller than that produced from tau-TEV256, and this size difference might facilitate its nuclear relocation, in line with the results shown in Fig. 7C.

Whatever the mechanism, nuclear relocalization of tau fragments might partly explain the deleterious effects of tau cleavage. The presence of full-length tau has previously been reported in nuclei from cultured cells and human brain cells (Loomis et al., 1990; Brady et al., 1995; Thurston et al., 1996; Cross et al., 2000; Sjoberg et al., 2006). Tau interacts with DNA and RNA and it has been proposed that it protects these molecules against denaturation and damage from free radicals (Multhaup et al., 2015; Bukar Maina et al., 2016; Mansuroglu et al., 2016). Several recent reports indicated that pathological tau impairs normal nuclear functions in at least four different ways: (i) aggregated abnormal tau binds to RNA molecules and perturbs the splicing machinery (Lester et al., 2021), (ii) pathogenic tau can cause toxic depletion of nuclear calcium (Mahoney et al., 2020), (iii) highly phosphorylated tau impairs the normal function of nuclear pore complexes (Eftekharzadeh et al., 2018) and (iv) nuclear membrane deformations and altered nucleocytoplasmic transport were found in human neurons bearing tau mutations related to frontotemporal dementia (Paonessa et al., 2019). In this context, the means by which pathological fragments of tau

Fig. 6. Relocalization of the N- and C-terminal fragments of tau with regards to the cytoskeleton after cleavage at site 256. (A, B) In CTRL condition (no cleavage), tau-TEV256 is localized on the microtubule cytoskeleton (**A**, arrowheads) or on both actin and microtubule cytoskeletons (**B**, arrows indicate localization on actin stress fibers, and arrowheads indicate localization on microtubules). **(C, D)** In CUT condition (after cleavage), the GFP N-terminal fragment was observed to enter the nucleus (stars). **(C)** In most cells, both GFP N-terminal and mCherry C-terminal fragments produced either diffuse staining in the cytosol or exhibited an actin-like pattern (arrows). **(D)** In ~10% of cells, like the one shown here, the two fragments adopted a dichotomous localization after cleavage, with the GFP N-terminal fragment on actin filaments (arrow) and the mCherry C-terminal fragment onto microtubules (arrowheads). Scale bars = 20 μm. **(E)** Quantification of localization patterns (as described in Fig. S1) exhibited by non-cleaved tau-TEV256 in control cells (CTRL), or by the GFP N-terminal fragment (CUT-GFP) or the mCherry C-terminal fragment (CUT-mCh) after cleavage. For the CUT condition, only cells exhibiting a green nucleus were examined. Cells were analyzed in two independent experiments (n = 400 for tau-TEV256 CTRL, n = 185 for CUT-GFP, and n = 295 for CUT-mCh). ***$P < 0.001$, Chi-square test.

Please cite this article in press as: Fourest-Lieuvin A et al. Controlled Tau Cleavage in Cells Reveals Abnormal Localizations of Tau Fragments. Neuroscience (2022), https://doi.org/10.1016/j.neuroscience.2022.08.016

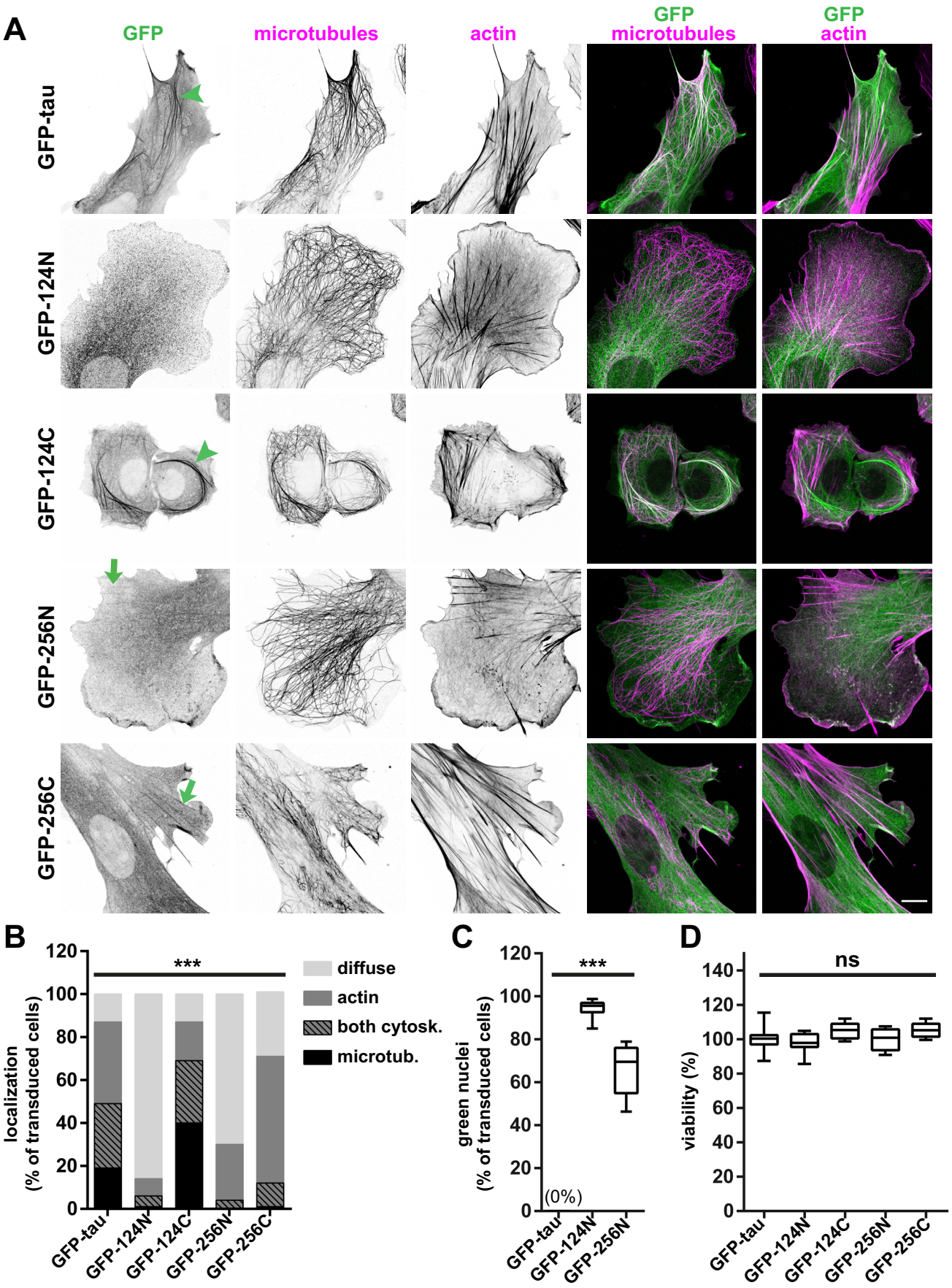
A
GFP
microtubules
actin
GFP microtubules
GFP actin
GFP-tau
GFP-124N
GFP-124C
GFP-256N
GFP-256C
B
localization (% of transduced cells)
***
diffuse
actin
both cytosk.
microtub.
GFP-tau
GFP-124N
GFP-124C
GFP-256N
GFP-256C
C
green nuclei (% of transduced cells)
***
(0%)
GFP-tau
GFP-124N
GFP-256N
D
viability (%)
ns
GFP-tau
GFP-124N
GFP-124C
GFP-256N
GFP-256C

impair nuclear homeostasis following invasion of the nucleus remains an open and interesting question.

Another striking observation following tau truncation was changes to cytoskeleton localization of some of the fragments released compared to non-cleaved tau, as illustrated by tau-TEV124 and tau-TEV256. In most control cells, non-cleaved tau-TEV124 and tau-TEV256 localize on microtubules or on both microtubules and actin, like the unmodified GFP-tau (compare Figs. 5D and 6E with Fig. 7B). However, when tau-TEV124 was cleaved, the N-terminal fragment in most cells displayed a diffuse staining pattern in the cytoplasm, combined with the nuclear relocalization mentioned above. The diffuse cytoplasmic pattern was expected, since the N-terminal fragment of tau-TEV124 corresponds to part of tau's projection domain, and lacks the cytoskeleton-binding domain (Fig. 1B). In contrast, the C-terminal fragment of tau-TEV124 contains all the sequences known to bind the actin and microtubule cytoskeletons (He et al., 2009; Elie et al., 2015; Cabrales Fontela et al., 2017). Nevertheless, this fragment was seen to interact more extensively with microtubules (Fig. 5D). Thus, it appears that the absence of part of the projection domain favors tau fragment binding to microtubules rather than to actin filaments.

Following tau-TEV256 cleavage, in some cells the N-terminal fragment exhibited a diffuse localization pattern, like that observed with the N-terminal fragment of tau-TEV124. The N-terminal tau-TEV256 fragment could also associate with actin filaments, probably via the P1 and P2 proline-rich motifs known to interact with actin (see Fig. 1B) (He et al., 2009). The C-terminal tau-TEV256 fragment showed an actin-like localization pattern in most of the cells examined. Although this fragment lacks the P1 and P2 motifs, it probably interacts with actin through the repeat domains which were shown to bind both actin and microtubules (Elie et al., 2015; Cabrales Fontela et al., 2017). Thus, tau cleavage at position 256 generates two fragments that both target actin filaments but exhibit a weak microtubular staining pattern. This conclusion concurs with those of previous studies reporting that the association of tau with microtubules in cells requires both tau repeats and the adjacent proline-rich sequences (Preuss et al., 1997).

Overall, the controlled tau cleavage system revealed altered cellular localization of tau fragments compared to that of the parental full-length tau. Furthermore, the simultaneous presence of both N- and C-terminal fragments appeared to be more toxic for cells than the sole expression of individual fragments (Figs. 3B and 7D). This effect might be explained by additive toxic effects of fragments on both the nucleus and cytoskeleton.

In conclusion, in this study we developed a cellular system to reproduce tau cleavage at specific sites found in AD patients' brains. We used this system to determine the fate and deleterious effects of the fragments released, in conditions close to the pathological context. Our results emphasize the importance of studying both nuclear damage and alterations to cytoskeletal regulation when seeking to decipher cellular dysfunction in tau-related pathologies.

ACKNOWLEDGEMENTS

We thank Yasmina Saoudi at the Photonic Imaging Center of Grenoble Institut Neurosciences (PIC-GIN), and Julie Brocard at the virus production facility for their help. This work was supported by INSERM, CEA, CNRS, Université Grenoble Alpes and by grants from the French Agence Nationale de la Recherche (2017-CE11-0026 MAMAs) and from the Union France Alzheimer et Maladies Apparentées and the Fédération pour la Recherche sur le Cerveau (FRC) (AAP SM 2015). A.V. was supported by the Union France Alzheimer et Maladies Apparentées and the Fédération pour la Recherche sur le Cerveau (FRC) (AAP SM 2015). The Photonic Imaging Center at Grenoble Institut Neurosciences (Univ. Grenoble Alpes – Inserm U1216) is part of the ISdV core facility and IBiSA-accredited. The Grenoble Institute of Neurosciences is part of the Grenoble Center of Excellence in Neurodegeneration (GREEN).

COMPETING INTEREST

The authors declare that they have no competing interests.

REFERENCES

Afreen S, Ferreira A (2019) Altered Cytoskeletal Composition and Delayed Neurite Elongation in tau45-230-Expressing Hippocampal Neurons. Neuroscience 412:1–15.

Afreen S, Riherd Methner DN, Ferreira A (2017) Tau45-230 association with the cytoskeleton and membrane-bound

Fig. 7. Cytoskeleton localization of N- and C-terminal tau fragments transduced individually into cells. (A) MEF cells were transduced with constructs coding for full-length GFP-tau or GFP-fragments of tau, indicated to the left of each panel, and stained with an anti-GFP antibody (first column), an anti-tubulin antibody (second column), and Atto 647-phalloidin (third column). Merged confocal airyscan images show the position of GFP-labeled proteins in relation to microtubules (fourth column) or actin (fifth column). These representative images show the main localization patterns for each protein fragment expressed. Arrowheads indicate GFP-labeled proteins localized on microtubules; arrows point to their localization on actin stress fibers. Scale bar = 10 μm. **(B)** Quantification of localization patterns (as described in Fig. S1) exhibited by full-length GFP-tau or each tau fragment. For each, 300 cells were analyzed from two independent experiments. ***$P < 0.001$, Chi-square test. **(C)** MEF cells transduced with full-length GFP-tau, GFP-124N or GFP-256N, were counted to determine the percentage of cells in which the nucleus was stained green. Number of counts performed in two independent experiments: $n = 5$ counts (a total of 256 cells examined) for GFP-tau, $n = 7$ counts (339 cells) for GFP-124N, and $n = 7$ counts (663 cells) for GFP-256N. ***$P < 0.001$, Kruskal-Wallis test. **(D)** MTT viability tests performed on MEF cells after three days of expression of full-length GFP-tau or of each tau fragment. Results were normalized by expressing them as a percentage of the mean for GFP-tau. Number of tests from two independent experiments: 12 for GFP-tau, 9 for GFP-124N, 9 for GFP-124C, 9 for GFP-256N, 8 for GFP-256C. ns, non-significant, Kruskal-Wallis test.

organelles: Functional implications in neurodegeneration. Neuroscience 362:104–117.
Biswas S, Kalil K (2018) The Microtubule-Associated Protein Tau Mediates the Organization of Microtubules and Their Dynamic Exploration of Actin-Rich Lamellipodia and Filopodia of Cortical Growth Cones. J Neurosci: Off J Soc Neurosci 38:291–307.
Bondulich MK, Guo T, Meehan C, Manion J, Rodriguez Martin T, Mitchell JC, Hortobagyi T, Yankova N, Stygelbout V, Brion JP, Noble W, Hanger DP (2016) Tauopathy induced by low level expression of a human brain-derived tau fragment in mice is rescued by phenylbutyrate. Brain: J Neurol 139:2290–2306.
Brady RM, Zinkowski RP, Binder LI (1995) Presence of tau in isolated nuclei from human brain. Neurobiol Aging 16:479–486.
Brandt R, Lee G (1993) Functional organization of microtubule-associated protein tau. Identification of regions which affect microtubule growth, nucleation, and bundle formation in vitro. J Biol Chem 268:3414–3419.
Bukar Maina M, Al-Hilaly YK, Serpell LC (2016) Nuclear tau and its potential role in Alzheimer's disease. Biomolecules 6:9.
Cabrales Fontela Y, Kadavath H, Biernat J, Riedel D, Mandelkow E, Zweckstetter M (2017) Multivalent cross-linking of actin filaments and microtubules through the microtubule-associated protein Tau. Nat Commun 8:1981.
Chen J, Kanai Y, Cowan NJ, Hirokawa N (1992) Projection domains of MAP2 and tau determine spacings between microtubules in dendrites and axons. Nature 360:674–677.
Cleveland DW, Hwo SY, Kirschner MW (1977a) Physical and chemical properties of purified tau factor and the role of tau in microtubule assembly. J Mol Biol 116:227–247.
Cleveland DW, Hwo SY, Kirschner MW (1977b) Purification of tau, a microtubule-associated protein that induces assembly of microtubules from purified tubulin. J Mol Biol 116:207–225.
Cook JA, Mitchell JB (1989) Viability measurements in mammalian cell systems. Anal Biochem 179:1–7.
Correas I, Padilla R, Avila J (1990) The tubulin-binding sequence of brain microtubule-associated proteins, tau and MAP-2, is also involved in actin binding. Biochem J 269:61–64.
Cross DC, Munoz JP, Hernandez P, Maccioni RB (2000) Nuclear and cytoplasmic tau proteins from human nonneuronal cells share common structural and functional features with brain tau. J Cell Biochem 78:305–317.
de Calignon A, Fox LM, Pitstick R, Carlson GA, Bacskai BJ, Spires-Jones TL, Hyman BT (2010) Caspase activation precedes and leads to tangles. Nature 464:1201–1204.
Deglon N, Tseng JL, Bensadoun JC, Zurn AD, Arsenijevic Y, Pereira de Almeida L, Zufferey R, Trono D, Aebischer P (2000) Self-inactivating lentiviral vectors with enhanced transgene expression as potential gene transfer system in Parkinson's disease. Hum Gene Ther 11:179–190.
Derisbourg M, Leghay C, Chiappetta G, Fernandez-Gomez FJ, Laurent C, Demeyer D, Carrier S, Buee-Scherrer V, Blum D, Vinh J, Sergeant N, Verdier Y, Buee L, Hamdane M (2015) Role of the Tau N-terminal region in microtubule stabilization revealed by new endogenous truncated forms. Sci Rep 5:9659.
d'Orange M, Auregan G, Cheramy D, Gaudin-Guerif M, Lieger S, Guillermier M, Stimmer L, Josephine C, Herard AS, Gaillard MC, Petit F, Kiessling MC, Schmitz C, Colin M, Buee L, Panayi F, Diguet E, Brouillet E, Hantraye P, Bemelmans AP, Cambon K (2018) Potentiating tangle formation reduces acute toxicity of soluble tau species in the rat. Brain: J Neurol 141:535–549.
Eftekharzadeh B, Daigle JG, Kapinos LE, Coyne A, Schiantarelli J, Carlomagno Y, Cook C, Miller SJ, Dujardin S, Amaral AS, Grima JC, Bennett RE, Tepper K, DeTure M, Vanderburg CR, Corjuc BT, DeVos SL, Gonzalez JA, Chew J, Vidensky S, Gage FH, Mertens J, Troncoso J, Mandelkow E, Salvatella X, Lim RYH, Petrucelli L, Wegmann S, Rothstein JD, Hyman BT (2018) Tau protein disrupts nucleocytoplasmic transport in Alzheimer's disease. Neuron 99:925–940.e927.
El-Daher MT, Hangen E, Bruyere J, Poizat G, Al-Ramahi I, Pardo R, Bourg N, Souquere S, Mayet C, Pierron G, Leveque-Fort S, Botas J, Humbert S, Saudou F (2015) Huntingtin proteolysis releases non-polyQ fragments that cause toxicity through dynamin 1 dysregulation. EMBO J 34:2255–2271.
Elie A, Prezel E, Guerin C, Denarier E, Ramirez-Rios S, Serre L, Andrieux A, Fourest-Lieuvin A, Blanchoin L, Arnal I (2015) Tau co-organizes dynamic microtubule and actin networks. Sci Rep 5:9964.
Farias GA, Munoz JP, Garrido J, Maccioni RB (2002) Tubulin, actin, and tau protein interactions and the study of their macromolecular assemblies. J Cell Biochem 85:315–324.
Fasulo L, Ugolini G, Visintin M, Bradbury A, Brancolini C, Verzillo V, Novak M, Cattaneo A (2000) The neuronal microtubule-associated protein tau is a substrate for caspase-3 and an effector of apoptosis. J Neurochem 75:624–633.
Fasulo L, Ugolini G, Cattaneo A (2005) Apoptotic effect of caspase-3 cleaved tau in hippocampal neurons and its potentiation by tau FTDP-mutation N279K. J Alzheimer's Dis: JAD 7:3–13.
Frandemiche ML, De Seranno S, Rush T, Borel E, Elie A, Arnal I, Lante F, Buisson A (2014) Activity-dependent tau protein translocation to excitatory synapse is disrupted by exposure to amyloid-beta oligomers. J Neurosci: Off J Soc Neurosci 34:6084–6097.
Fulga TA, Elson-Schwab I, Khurana V, Steinhilb ML, Spires TL, Hyman BT, Feany MB (2007) Abnormal bundling and accumulation of F-actin mediates tau-induced neuronal degeneration in vivo. Nat Cell Biol 9:139–148.
Gamblin TC, Chen F, Zambrano A, Abraha A, Lagalwar S, Guillozet AL, Lu M, Fu Y, Garcia-Sierra F, LaPointe N, Miller R, Berry RW, Binder LI, Cryns VL (2003) Caspase cleavage of tau: linking amyloid and neurofibrillary tangles in Alzheimer's disease. PNAS 100:10032–10037.
Gray DC, Mahrus S, Wells JA (2010) Activation of specific apoptotic caspases with an engineered small-molecule-activated protease. Cell 142:637–646.
Guo T, Noble W, Hanger DP (2017) Roles of tau protein in health and disease. Acta Neuropathol 133:665–704.
Guo T, Dakkak D, Rodriguez-Martin T, Noble W, Hanger DP (2019) A pathogenic tau fragment compromises microtubules, disrupts insulin signaling and induces the unfolded protein response. Acta Neuropathol Commun 7:2.
He HJ, Wang XS, Pan R, Wang DL, Liu MN, He RQ (2009) The proline-rich domain of tau plays a role in interactions with actin. BMC Cell Biol 10:81.
Kanai Y, Chen J, Hirokawa N (1992) Microtubule bundling by tau proteins in vivo: analysis of functional domains. EMBO J 11:3953–3961.
Kapitein LC, Hoogenraad CC (2015) Building the neuronal microtubule cytoskeleton. Neuron 87:492–506.
Kempf M, Clement A, Faissner A, Lee G, Brandt R (1996) Tau binds to the distal axon early in development of polarity in a microtubule- and microfilament-dependent manner. J Neurosci: Off J Soc Neurosci 16:5583–5592.
Lester E, Ooi FK, Bakkar N, Ayers J, Woerman AL, Wheeler J, Bowser R, Carlson GA, Prusiner SB, Parker R (2021) Tau aggregates are RNA-protein assemblies that mislocalize multiple nuclear speckle components. Neuron 109:1675–1691.e1679.
Loomis PA, Howard TH, Castleberry RP, Binder LI (1990) Identification of nuclear tau isoforms in human neuroblastoma cells. PNAS 87:8422–8426.
Mahoney R, Ochoa Thomas E, Ramirez P, Miller HE, Beckmann A, Zuniga G, Dobrowolski R, Frost B (2020) Pathogenic tau causes a toxic depletion of nuclear calcium. Cell Rep 32:107900.
Mansuroglu Z, Benhelli-Mokrani H, Marcato V, Sultan A, Violet M, Chauderlier A, Delattre L, Loyens A, Talahari S, Begard S, Nesslany F, Colin M, Soues S, Lefebvre B, Buee L, Galas MC, Bonnefoy E (2016) Loss of Tau protein affects the structure, transcription and repair of neuronal pericentromeric heterochromatin. Sci Rep 6:33047.
Martinisi A, Flach M, Sprenger F, Frank S, Tolnay M, Winkler DT (2021) Severe oligomeric tau toxicity can be reversed without long-term sequelae. Brain: J Neurol 144:963–974.

Matsumoto SE, Motoi Y, Ishiguro K, Tabira T, Kametani F, Hasegawa M, Hattori N (2015) The twenty-four KDa C-terminal tau fragment increases with aging in tauopathy mice: implications of prion-like properties. Hum Mol Genet 24:6403–6416.

Moraga DM, Nunez P, Garrido J, Maccioni RB (1993) A tau fragment containing a repetitive sequence induces bundling of actin filaments. J Neurochem 61:979–986.

Multhaup G, Huber O, Buee L, Galas MC (2015) Amyloid Precursor Protein (APP) Metabolites APP Intracellular Fragment (AICD), Abeta42, and tau in nuclear roles. J Biol Chem 290:23515–23522.

Novak P, Cehlar O, Skrabana R, Novak M (2018) Tau conformation as a target for disease-modifying therapy: The role of truncation. J. Alzheimer's Dis.: JAD 64:S535–S546.

Ozcelik S, Sprenger F, Skachokova Z, Fraser G, Abramowski D, Clavaguera F, Probst A, Frank S, Muller M, Staufenbiel M, Goedert M, Tolnay M, Winkler DT (2016) Co-expression of truncated and full-length tau induces severe neurotoxicity. Mol Psychiatry 21:1790–1798.

Paholikova K, Salingova B, Opattova A, Skrabana R, Majerova P, Zilka N, Kovacech B, Zilkova M, Barath P, Novak M (2015) N-terminal truncation of microtubule associated protein tau dysregulates its cellular localization. J Alzheimer's Dis: JAD 43:915–926.

Paonessa F, Evans LD, Solanki R, Larrieu D, Wray S, Hardy J, Jackson SP, Livesey FJ (2019) Microtubules deform the nuclear membrane and disrupt nucleocytoplasmic transport in tau-mediated frontotemporal dementia. Cell Rep 26:582–593.e585.

Park SY, Ferreira A (2005) The generation of a 17 kDa neurotoxic fragment: an alternative mechanism by which tau mediates beta-amyloid-induced neurodegeneration. J Neurosci: Off J Soc Neurosci 25:5365–5375.

Patterson KR, Remmers C, Fu Y, Brooker S, Kanaan NM, Vana L, Ward S, Reyes JF, Philibert K, Glucksman MJ, Binder LI (2011) Characterization of prefibrillar Tau oligomers in vitro and in Alzheimer disease. J Biol Chem 286:23063–23076.

Peris L, Thery M, Faure J, Saoudi Y, Lafanechere L, Chilton JK, Gordon-Weeks P, Galjart N, Bornens M, Wordeman L, Wehland J, Andrieux A, Job D (2006) Tubulin tyrosination is a major factor affecting the recruitment of CAP-Gly proteins at microtubule plus ends. J Cell Biol 174:839–849.

Preuss U, Biernat J, Mandelkow EM, Mandelkow E (1997) The 'jaws' model of tau-microtubule interaction examined in CHO cells. J Cell Sci 110(Pt 6):789–800.

Prezel E, Elie A, Delaroche J, Stoppin-Mellet V, Bosc C, Serre L, Fourest-Lieuvin A, Andrieux A, Vantard M, Arnal I (2018) Tau can switch microtubule network organizations: from random networks to dynamic and stable bundles. Mol Biol Cell 29:154–165.

Quinn JP, Corbett NJ, Kellett KAB, Hooper NM (2018) Tau proteolysis in the pathogenesis of tauopathies: neurotoxic fragments and novel biomarkers. J Alzheimer's Dis: JAD 63:13–33.

Ramirez-Rios S, Denarier E, Prezel E, Vinit A, Stoppin-Mellet V, Devred F, Barbier P, Peyrot V, Sayas CL, Avila J, Peris L, Andrieux A, Serre L, Fourest-Lieuvin A, Arnal I (2016) Tau antagonizes end-binding protein tracking at microtubule ends through a phosphorylation-dependent mechanism. Mol Biol Cell 27:2924–2934.

Samsonov A, Yu JZ, Rasenick M, Popov SV (2004) Tau interaction with microtubules in vivo. J Cell Sci 117:6129–6141.

Sjoberg MK, Shestakova E, Mansuroglu Z, Maccioni RB, Bonnefoy E (2006) Tau protein binds to pericentromeric DNA: a putative role for nuclear tau in nucleolar organization. J Cell Sci 119:2025–2034.

Sohn PD, Huang CT, Yan R, Fan L, Tracy TE, Camargo CM, Montgomery KM, Arhar T, Mok SA, Freilich R, Baik J, He M, Gong S, Roberson ED, Karch CM, Gestwicki JE, Xu K, Kosik KS, Gan L (2019) Pathogenic Tau impairs axon initial segment plasticity and excitability homeostasis. Neuron 104:458–470.e455.

Takeda S, Wegmann S, Cho H, DeVos SL, Commins C, Roe AD, Nicholls SB, Carlson GA, Pitstick R, Nobuhara CK, Costantino I, Frosch MP, Muller DJ, Irimia D, Hyman BT (2015) Neuronal uptake and propagation of a rare phosphorylated high-molecular-weight tau derived from Alzheimer's disease brain. Nat Commun 6:8490.

Takemura R, Okabe S, Umeyama T, Kanai Y, Cowan NJ, Hirokawa N (1992) Increased microtubule stability and alpha tubulin acetylation in cells transfected with microtubule-associated proteins MAP1B, MAP2 or tau. J Cell Sci 103(Pt 4):953–964.

Tan YS, Lei YL (2019) Generation and Culture of Mouse Embryonic Fibroblasts. Methods Mol Biol 1960:85–91.

Thurston VC, Zinkowski RP, Binder LI (1996) Tau as a nucleolar protein in human nonneural cells in vitro and in vivo. Chromosoma 105:20–30.

Timney BL, Raveh B, Mironska R, Trivedi JM, Kim SJ, Russel D, Wente SR, Sali A, Rout MP (2016) Simple rules for passive diffusion through the nuclear pore complex. J Cell Biol 215:57–76.

Torres-Cruz FM, Rodriguez-Cruz F, Escobar-Herrera J, Barragan-Andrade N, Basurto-Islas G, Ripova D, Avila J, Garcia-Sierra F (2016) Expression of Tau produces aberrant plasma membrane blebbing in glial cells through RhoA-ROCK-dependent F-actin remodeling. J Alzheimer's Dis: JAD 52:463–482.

Wehr MC, Laage R, Bolz U, Fischer TM, Grunewald S, Scheek S, Bach A, Nave KA, Rossner MJ (2006) Monitoring regulated protein-protein interactions using split TEV. Nat Methods 3:985–993.

Weingarten MD, Lockwood AH, Hwo SY, Kirschner MW (1975) A protein factor essential for microtubule assembly. PNAS 72:1858–1862.

Wray S, Saxton M, Anderton BH, Hanger DP (2008) Direct analysis of tau from PSP brain identifies new phosphorylation sites and a major fragment of N-terminally cleaved tau containing four microtubule-binding repeats. J Neurochem 105:2343–2352.

Yu JZ, Rasenick MM (2006) Tau associates with actin in differentiating PC12 cells. FASEB J: Off Publ Fed Am Soc Exp Biol 20:1452–1461.

Zempel H, Dennissen FJA, Kumar Y, Luedtke J, Biernat J, Mandelkow EM, Mandelkow E (2017) Axodendritic sorting and pathological missorting of Tau are isoform-specific and determined by axon initial segment architecture. J Biol Chem 292:12192–12207.

Zhang Z, Song M, Liu X, Kang SS, Kwon IS, Duong DM, Seyfried NT, Hu WT, Liu Z, Wang JZ, Cheng L, Sun YE, Yu SP, Levey AI, Ye K (2014) Cleavage of tau by asparagine endopeptidase mediates the neurofibrillary pathology in Alzheimer's disease. Nat Med 20:1254–1262.

Zhao X, Kotilinek LA, Smith B, Hlynialuk C, Zahs K, Ramsden M, Cleary J, Ashe KH (2016) Caspase-2 cleavage of tau reversibly impairs memory. Nat Med 22:1268–1276.

Zhou L, McInnes J, Wierda K, Holt M, Herrmann AG, Jackson RJ, Wang YC, Swerts J, Beyens J, Miskiewicz K, Vilain S, Dewachter I, Moechars D, De Strooper B, Spires-Jones TL, De Wit J, Verstreken P (2017) Tau association with synaptic vesicles causes presynaptic dysfunction. Nat Commun 8:15295.

Zilka N, Filipcik P, Koson P, Fialova L, Skrabana R, Zilkova M, Rolkova G, Kontsekova E, Novak M (2006) Truncated tau from sporadic Alzheimer's disease suffices to drive neurofibrillary degeneration in vivo. FEBS Lett 580:3582–3588.

APPENDIX A. SUPPLEMENTARY MATERIAL

Supplementary material to this article can be found online at https://doi.org/10.1016/j.neuroscience.2022.08.016.

(Received 16 December 2021, Accepted 16 August 2022)
(Available online xxxx)